Supplementary Information

Bio-skin inspired 3D porous cellulose/$AlPO_4$ nano-laminated film with structure-enhanced selective emission for all-day non-power cooling

Shuangjiang Feng[1], Yuming Zhou[1*], Xi Chen[1], Shengnan Shi[1], Chenghuan Liu[1], Tao Zhang[2*]

[1]School of Chemistry and Chemical Engineering, Southeast University, Nanjing 211100, Jiangsu Province, China

[2]School of Chemistry and Chemical Engineering, Jiangsu University, Zhenjiang 212013, Jiangsu Province, China[1]

*Corresponding authors:

Tel./fax: +86 025 52090617.

E-mail: ymzhou@seu.edu.cn (Y, Zhou)

zhangtaochem@163.com (T, Zhang)

Content

Methodology

The average hemispherical emissivity ε from λ_1 to λ_2 is calculated by:

$$\varepsilon_{(\lambda_1-\lambda_2)} = \frac{\int_{\lambda_1}^{\lambda_2} eI_{BB}(\lambda)d\lambda}{\int_{\lambda_1}^{\lambda_2} I_{BB}(\lambda)d\lambda} \approx \frac{\sum_{\lambda_1}^{\lambda_2} \varepsilon_n}{n_2 - n_1 + 1} \quad (1)$$

Where I_{BB} is the radiance of the blackbody, T=298 K.

The average reflectivity in UV-vis-NIR is defined using the following equation:

$$R_{(0.3-2.5)} = \frac{\int_{0.3}^{2.5} R(\lambda)E(\lambda)d\lambda}{\int_{0.3}^{2.5} E(\lambda)d\lambda} R_{(0.3-2.5)} = \frac{\int_{0.3}^{2.5} R(\lambda)E(\lambda)d\lambda}{\int_{0.3}^{2.5} E(\lambda)d\lambda}$$

(2)

Where R(λ) is the reflectivity of membrane and E(λ) is the solar spectral irradiance profile as the function of wavelength.

Models and simulation

To demonstrate the interaction between different solvents and polymer, we perform the density functional theory (DFT) calculations. The simulation is performed with the density functional theory program DMol^3 in Material Studio. The physical wave functions are expanded in terms of numerical basis sets (Dmol^3/GGA-PBE/DNP(3.5) basis set). The exchange-correlation energy was calculated with Perdew-Burke-Ernzerhof (PBE) generalized gradient approximation (GGA). A Fermi smearing of 0.005 Ha (1 Ha = 27.211 eV) and a global orbital cutoff of 5.2 Å are employed. The convergence criteria for the geometric optimization and energy calculation are set as follows: (a) a self-consistent field tolerance of 1.0×10^{-6} Ha/atom; (b) an energy tolerance of 1.0×10^{-5} Ha/atom.

The solar radiation scattering models could be simulated with Finite difference time domain method (FDTD) and the scattering models included the cavities and inorganic nanoparticles was set as follows：

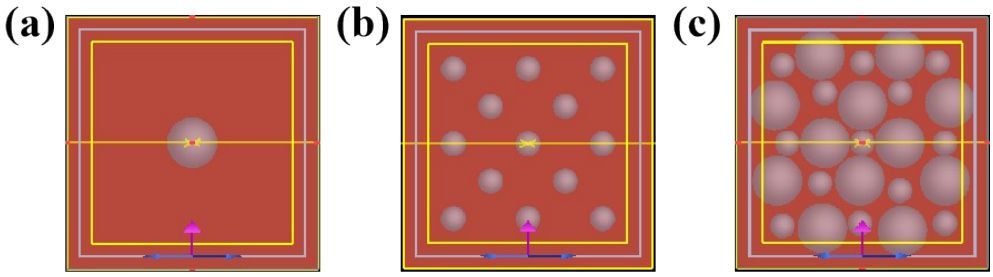

The images of models represented (a) single cavity; (b) multiple cavities; (c) multi-size hybrid cavities.

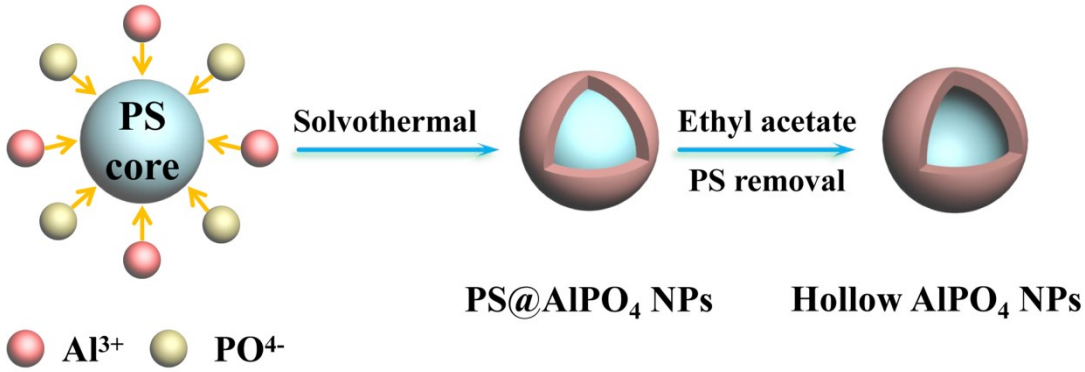

Fig.S1. Schematic illustration for the fabrication of hollow $AlPO_4$ nanoparticles.

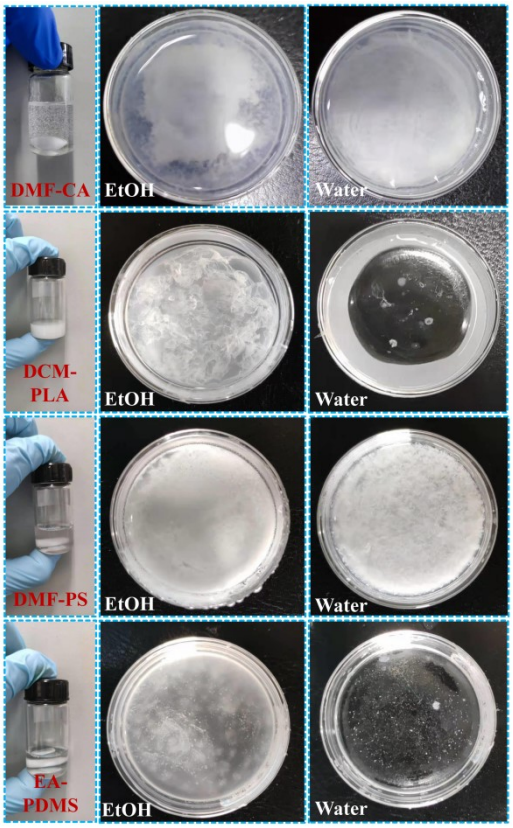

Fig.S2. Selected DMF as high-quality solvent of CA and the ultra-rapid extraction by inferior solvents and other examples of ultra-rapid polymer precipitation through solvent extraction inspired by solvents polarity matching.

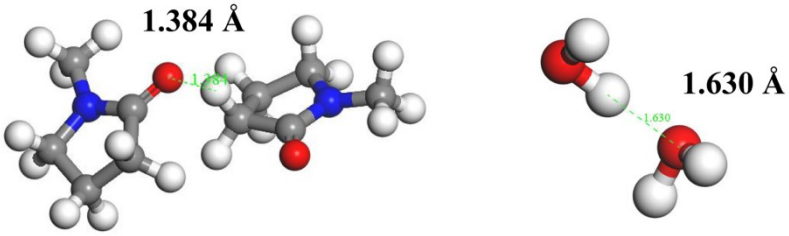

NMP-NMP **H_2O-H_2O**

Interacting molecules	Interaction energy (kcal/mol)
NMP-NMP	-2.1147
H_2O-H_2O	-7.4674
NMP-H_2O	-10.3602

Fig.S3. DFT models for solvents molecules and their interaction energy.

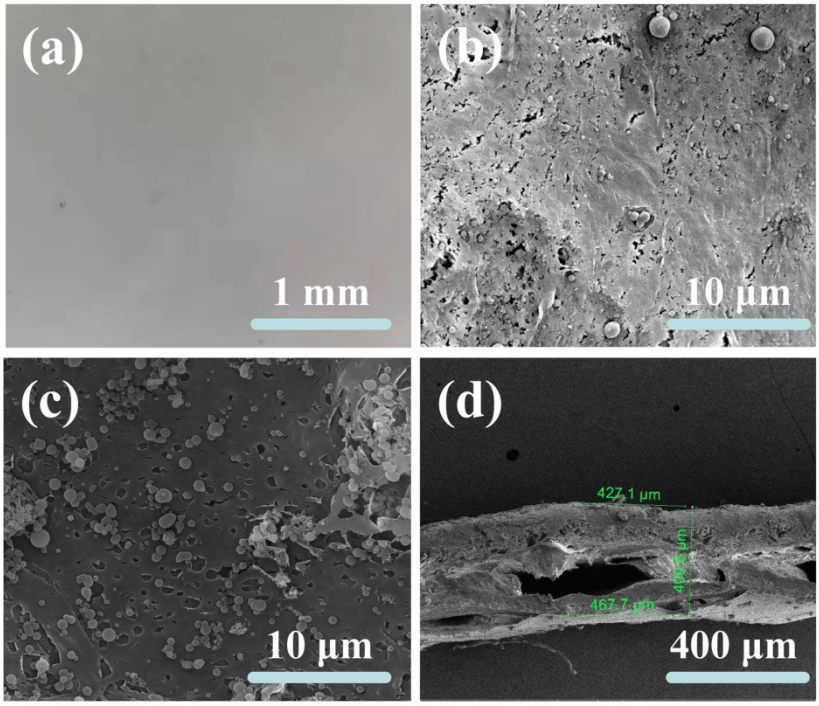

Fig.S4. (a) Macro optical photo of the bio-skin structural 3D PCA/h-$AlPO_4$ PRC film with smooth surface; SEM images (b) smooth surface, (c) wrinkle surface, (d) thickness of 3D PCA PRC film without dense nano-layer.

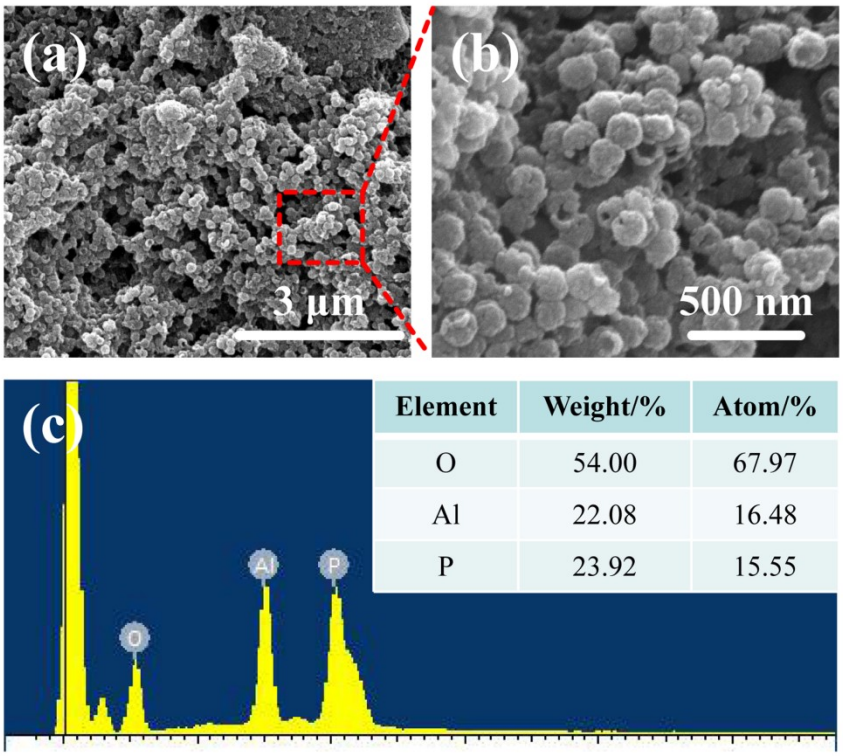

Element	Weight/%	Atom/%
O	54.00	67.97
Al	22.08	16.48
P	23.92	15.55

Fig.S5. SEM images of (a) (b) h-$AlPO_4$ nanoparticles and (c) EDS spectra.

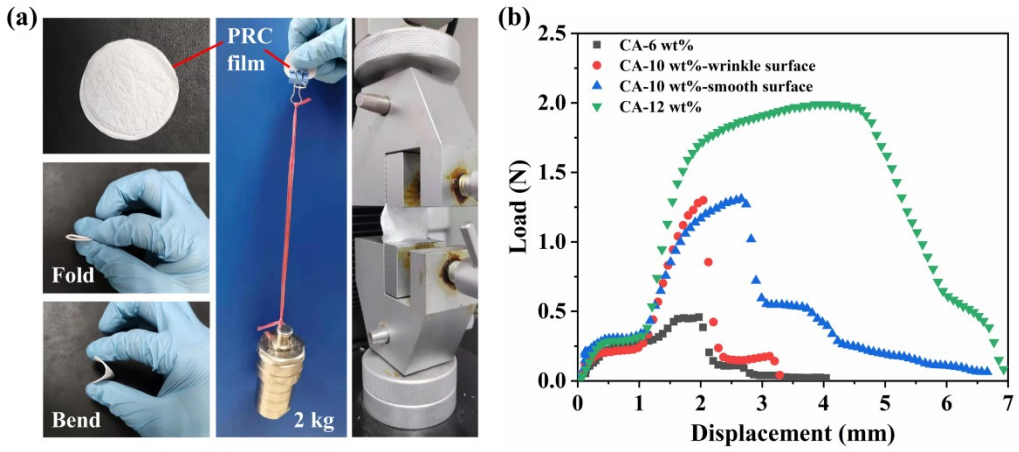

Fig.S6. Mechanical deformation and strength of the 3D PCA based PRC films.

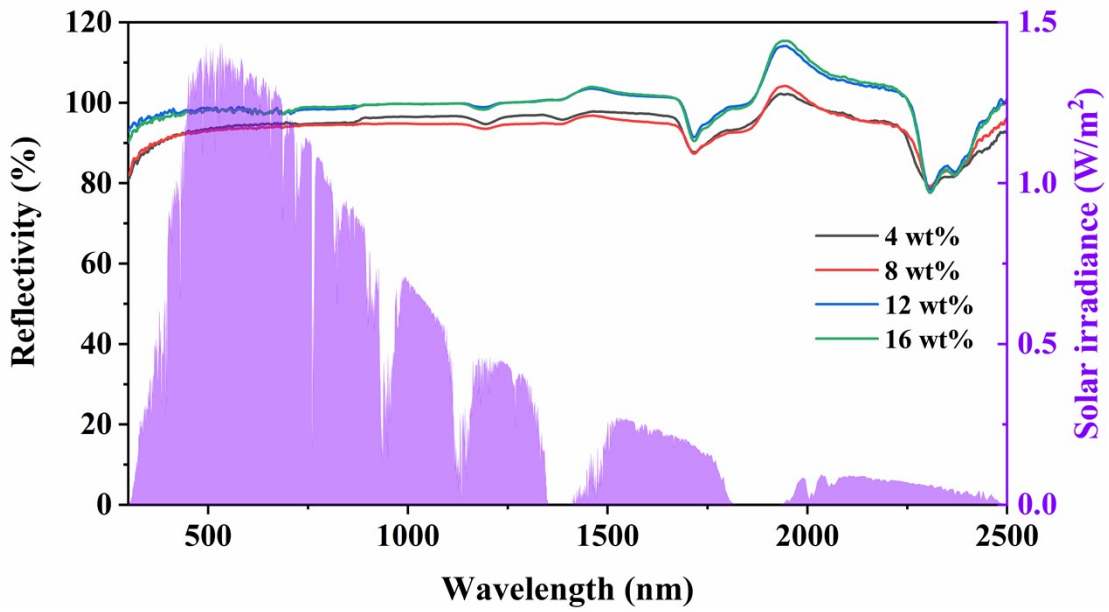

Fig.S7. Reflectance spectra of 3D PCA films with different concentrations of CA.

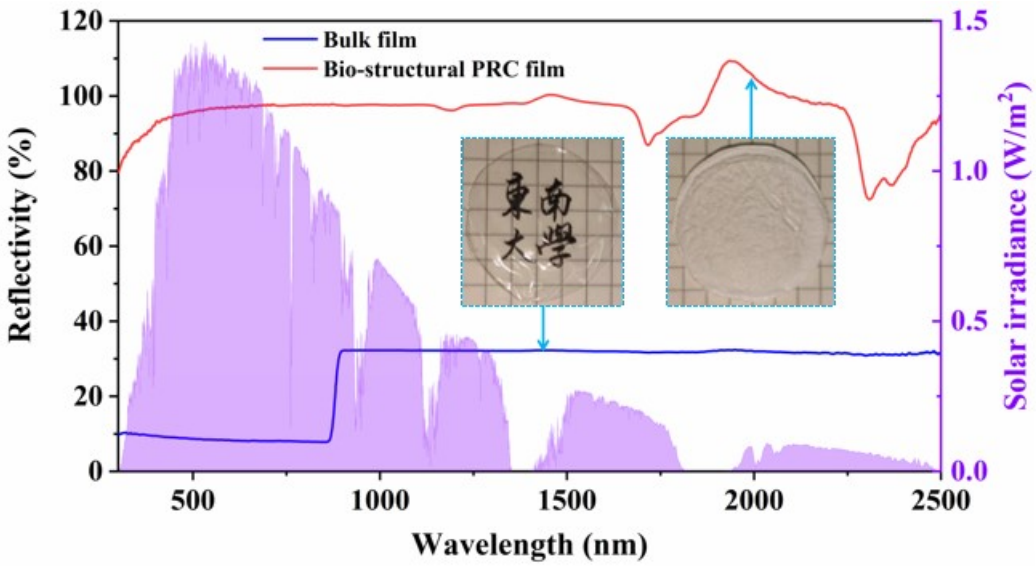

Fig.S8. Reflectance spectra of PCA based films with different internal structures including bulk and porous structures.

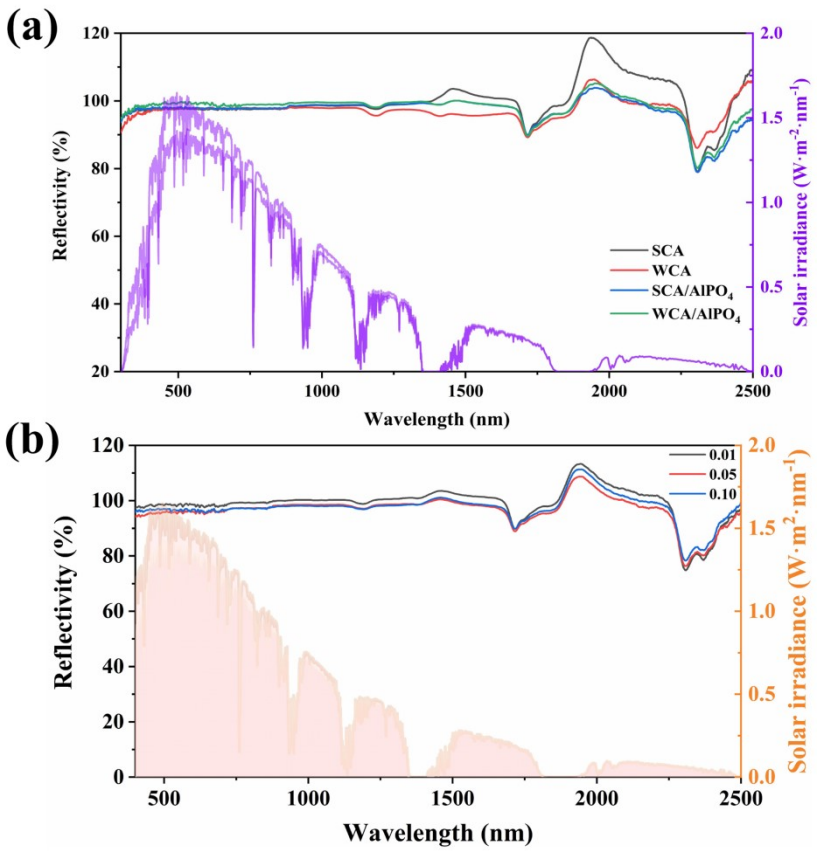

Fig.S9. Reflectance spectra (a) 3D PCA films with different surface morphology and deposited with h-$AlPO_4$ nanoparticles; (b) 3D PCA/h-$AlPO_4$ films deposited with different masses of nanoparticles.

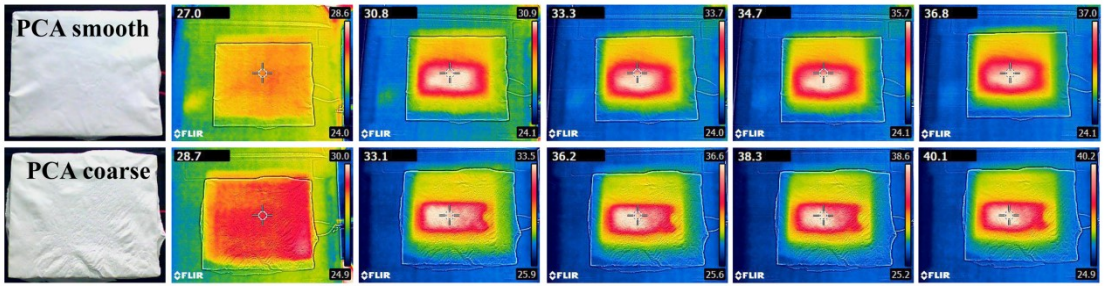

Fig.S10. Infrared emissivity reflected by infrared thermal imaging of 3D PCA films with different surface morphology.

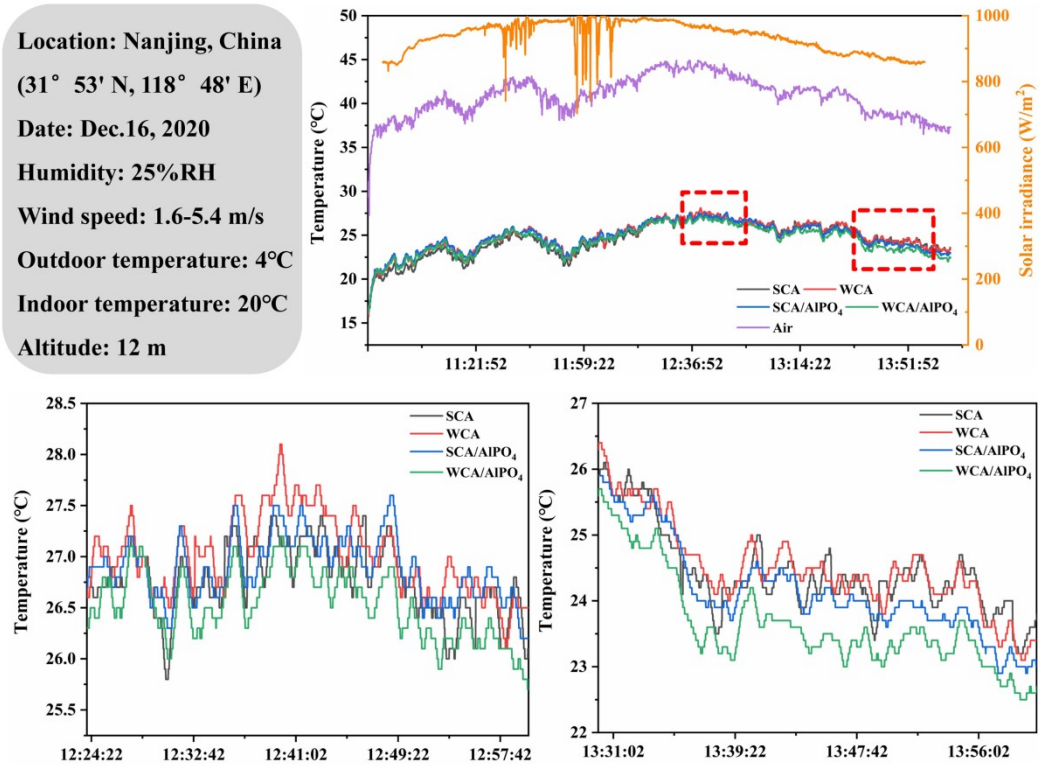

Fig.S11. Daytime outdoor PRC capacity of 3D PCA PRC films with different surface morphology under low environment temperature.

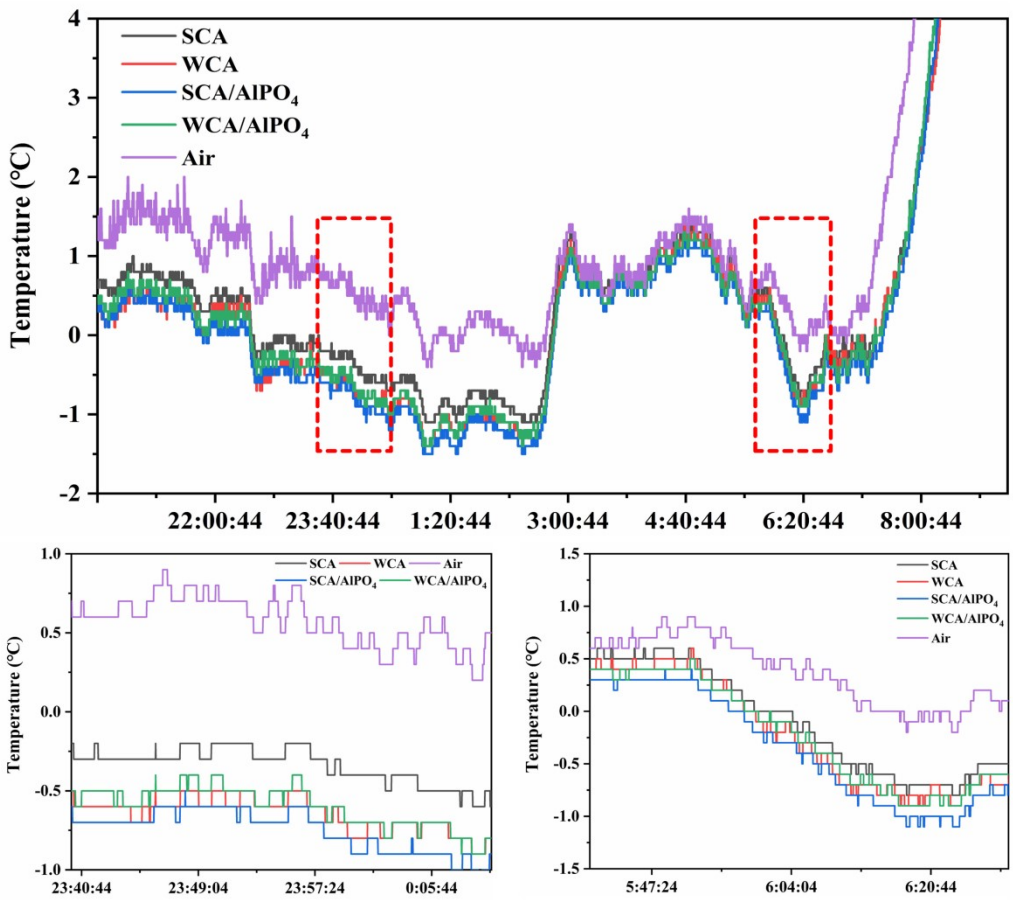

Fig.S12. Nighttime PRC capacity of 3D PCA films with different surface morphology and deposited with h-$AlPO_4$.

Table S1 Average solar radiation reflectivity and emissivity of PCA based PRC films.

Materials	R_{solar} (average %)	ε_{MIR} (average %)
3D PCA/h-$AlPO_4$-F-Wrinkle	97	94.7
3D PCA/h-$AlPO_4$-F-Smooth	95	88.7
3D PCA/h-$AlPO_4$-B	94	96.6